

Testing the continuum-discretized coupled channels method for deuteron-induced reactionsN. J. Upadhyay,¹ A. Deltuva,² and F. M. Nunes^{1,3}¹*National Superconducting Cyclotron Laboratory, Michigan State University, East Lansing, Michigan 48824-1321, USA*²*Centro de Física Nuclear da Universidade de Lisboa, P-1649-003 Lisboa, Portugal*³*Department of Physics and Astronomy, Michigan State University, East Lansing, Michigan 48824-1321, USA*

(Received 24 December 2011; revised manuscript received 4 March 2012; published 25 May 2012)

The continuum-discretized coupled channels (CDCC) method is a well established theory for direct nuclear reactions which includes breakup to all orders. Alternatively, the three-body problem can be solved exactly within the Faddeev formalism which explicitly includes breakup and transfer channels to all orders. With the aim to understand how CDCC compares with the exact three-body Faddeev formulation, we study deuteron-induced reactions on (i) ^{10}Be at $E_d = 21.4, 40.9$ and 71 MeV; (ii) ^{12}C at $E_d = 12$ and 56 MeV; and (iii) ^{48}Ca at $E_d = 56$ MeV. We calculate elastic, transfer, and breakup cross sections. Overall, the discrepancies found for elastic scattering are small with the exception of very backward angles. For transfer cross sections at low energy, ~ 10 MeV/u, CDCC is in good agreement with the Faddeev-type results and the discrepancy increases with beam energy. In contrast, breakup observables obtained with CDCC are in good agreement with Faddeev-type results for all but the lower energies considered here.

DOI: [10.1103/PhysRevC.85.054621](https://doi.org/10.1103/PhysRevC.85.054621)

PACS number(s): 24.10.Ht, 24.10.Eq, 25.55.Hp

I. INTRODUCTION

The construction and upgrade of various radioactive beam facilities worldwide continues to open up new avenues for the study of direct nuclear reactions involving rare isotopes [1,2]. In the low-energy regime (around 10–20 MeV/u) one can explore the structure of the exotic nucleus in detail. Single neutron transfer using (p, d) or (d, p) is also becoming a common tool to explore neutron capture for astrophysics (e.g., Ref. [3]).

Given the long history of using deuteron-induced reactions (in normal kinematics) for studying nuclear structure, a number of reaction theories are well established. With the understanding that breakup strongly affects the reaction mechanism when the loosely bound deuteron is involved, theories including deuteron breakup were developed [4–6]. However, until recently the accuracy of these methods had not been quantified.

Faddeev devised a method which couples elastic, rearrangement, and breakup channels [7] by expanding the three-body wave function into three components. For any given three-body Hamiltonian, the Faddeev method provides the exact solution. For few-nucleon reactions an integral equation formulation for the transition operators [8,9] proposed by Alt, Grassberger, and Sandhas (AGS) is commonly used in the momentum-space framework. One critical issue in this method is the well known Coulomb problem. Screening and renormalization techniques [10,11] have been developed to handle the Coulomb problem, which opened the path for applications to deuteron-induced nuclear reactions [12,13]. This method can now be used to benchmark existing nuclear reaction theories.

One method of practical use in (d, p) and (p, d) reactions is the finite-range adiabatic wave approximation (ADWA) method [5], which takes into account deuteron breakup to all orders in the transfer channel while making an important simplification of the continuum. ADWA has been studied in detail in [14] and compared to exact Faddeev predictions in Refs. [15,16].

ADWA is the precursor of the continuum-discretized coupled channels (CDCC) method [6], which does not make approximations in the treatment of the breakup states. While ADWA provides a method to compute transfer alone, CDCC can be used for all: elastic scattering, breakup, and transfer. CDCC is now a standard tool to study deuteron-induced breakup reactions [17]. In CDCC, the three-body scattering problem is solved through a set of coupled Schrödinger-like differential equations. The breakup is included to all orders by expanding the full three-body wave function in terms of a complete basis of the projectile's bound and continuum states. A discretization by averaging over energy is common to handle the coupling between the continuum states. In addition to elastic scattering and breakup, attempts have been made to study transfer reactions using the CDCC wave function [12,18–21]. In these methods, the exact three-body wave function in the transfer amplitude is replaced by the CDCC wave function. Thus, starting from one single three-body Hamiltonian, CDCC can provide elastic, breakup, and transfer cross sections, although to some extent not all channels are treated on equal footing.

In theory, CDCC should provide an exact solution to the three-body problem. In practice, due to the truncation of the model space and discretization of the continuum into bins, this may not be true. For example, it is easy to demonstrate that the truncated deuteron CDCC wave function does not provide the correct asymptotic form for a bound state in a rearrangement channel. A first attempt to compare CDCC and Faddeev was performed in Ref. [12]. Good agreement was found for elastic scattering and breakup for deuterons on ^{12}C and ^{58}Ni while disagreement was observed for ^{11}Be on protons at $E = 38$ MeV/u in both breakup and transfer observables. The reaction calculations for ^{12}C and ^{58}Ni did not include bound states in the rearrangement channels and therefore one may naively expect the CDCC solution to provide the correct answer to the problem. The disagreement found for the single reaction where a bound transfer state was included, questioned the reliability of CDCC and called for a more systematic study.

The aim of this work is to quantify the accuracy of CDCC in computing elastic, breakup, and transfer cross sections, and to establish a range of validity. This will be done by direct comparison with exact Faddeev-AGS calculations (FAGS). Our test cases include deuteron scattering from ^{10}Be , ^{12}C , and ^{48}Ca . These reactions are studied as a function of beam energy, chosen to match available experimental data.

In Sec. II, we describe the details of the CDCC and AGS formalisms. In Sec. III we present the numerical details of the calculations, followed by the results and discussions in Sec. IV. Finally, the summary and conclusions are given in Sec. V.

II. FORMALISM

For describing the $A(d, d)A$, $A(d, p)B$, and $A(d, pn)A$ reactions we consider an effective three-body problem $p + n + A$, such that B is the ground state $B = n + A$. The Hamiltonian is then written as

$$H_{3b} = \hat{T}_R + \hat{T}_r + U_{pA} + U_{nA} + V_{pn}, \quad (1)$$

where the kinetic energy operators \hat{T}_R and \hat{T}_r can be expressed in any of the three Jacobi coordinate pairs [22]. The deuteron is modeled by a real potential, V_{pn} , reproducing its binding energy and the np 3S_1 low-energy phase shifts. The p - A and n - A interactions are phenomenological optical potentials, U_{pA} and U_{nA} , respectively. They include absorption from all the channels which are otherwise not included in the model space.

A. The CDCC method

In the CDCC approach, using the above mentioned three-body Hamiltonian [Eq. (1)], the three-body wave equation of the total system is written as

$$[H_{3b} - E] \Psi^{\text{CDCC}}(\mathbf{r}, \mathbf{R}) = \mathbf{0}, \quad (2)$$

where \mathbf{r} and \mathbf{R} are the Jacobi coordinates for the p - n and d - A systems, respectively. Here E is the total energy of the system in the center of mass (c.m.) frame.

Keeping in mind that the deuteron is a loosely bound system, we consider deuteron breakup states explicitly. The eigenstates of the deuteron, $\phi(\mathbf{r})$, satisfy the eigenvalue equation $(T_r + V_{np})\phi(\mathbf{r}) = \epsilon\phi(\mathbf{r})$. To reduce the computational cost, in this work we ignore the spins of the particles. We perform the standard partial wave decomposition in terms of the orbital angular momentum of the neutron relative to the proton (l) and the discretization of the deuteron continuum (indexed i) by slicing the continuum into bins and averaging over momentum [6,17,22]. In this manner, the projectile is represented by

$$\phi_i(\mathbf{r}) = \sum_l i^l \frac{u_{il}(r)}{r} Y_l(\hat{\mathbf{r}}), \quad (3)$$

where $i = 0$ refers to the deuteron ground state and $i > 0$ to the np continuum bin i corresponding to momentum $k_i = \sqrt{2\mu_{pn}\epsilon_i/\hbar^2}$ with μ_{pn} being the reduced mass of proton and neutron. The projectile continuum is truncated by restricting the orbital momentum ($l \leq l_{\text{max}}$) and the energy of the np

breakup bins ($\epsilon_i \leq \epsilon_{\text{max}}$). The limits are chosen such that the observables of interest are converged.

A partial wave decomposition in terms of the relative angular momentum between projectile and target (L) is also performed. Thus, the full three-body CDCC wave function can be written as

$$\Psi^{\text{CDCC}}(\mathbf{r}, \mathbf{R}) = \sum_{\alpha} i^{l+L} \frac{u_{i\alpha}(r)}{r} \chi_{\alpha}(R) Y_{l_{\alpha}}(\hat{\mathbf{r}}) Y_{L_{\alpha}}(\hat{\mathbf{R}}), \quad (4)$$

where we use α as a general index representing the quantum numbers $\alpha = \{iLL\}$.

Substituting Eq. (4) in Eq. (2), a set of coupled-channel equations is obtained for $\chi_{\alpha}(R)$,

$$\left[-\frac{\hbar^2}{2\mu_{dA}} \left(\frac{d^2}{dR^2} - \frac{L(L+1)}{R^2} \right) + V_{\alpha\alpha}(R) + \epsilon_i - E \right] \chi_{\alpha}(R) + \sum_{\alpha' \neq \alpha} i^{L'-L} V_{\alpha\alpha'}(R) \chi_{\alpha'}(R) = 0, \quad (5)$$

where μ_{dA} is the reduced mass of $d + A$, and $E_{\alpha} = E - \epsilon_i$. Equation (5) is solved with the scattering boundary conditions for large R :

$$\chi_{\alpha}(R) \rightarrow i/2 [H_{\alpha}^{-}(KR) \delta_{\alpha\alpha_i} - H_{\alpha}^{+}(KR) S_{\alpha\alpha_i}]. \quad (6)$$

Here, H^{-} and H^{+} are the Coulomb Hankel functions [22] and $S_{\alpha\alpha_i}$ is the S matrix. The coupling potentials in Eq. (5) are defined by

$$V_{\alpha\alpha'}(R) = \langle \phi_{il}(r) | U_{pA} + U_{nA} | \phi_{i'l'}(r) \rangle, \quad (7)$$

and contain both nuclear and Coulomb parts, which are expanded in terms of multipoles Q up to Q_{max} .

As mentioned before, the CDCC wave function Eq. (4) can be used in the exact transition amplitude for $A(d, p)B$. The post form for the transition amplitude is then

$$T = \langle \chi_{pB}^{(-)} \phi_{nA} | V_{pn} + U_{pA} - U_{pB} | \Psi^{\text{CDCC}} \rangle, \quad (8)$$

where $\chi_{pB}^{(-)}$ is the distorted wave generated by the auxiliary potential U_{pB} (depending on \mathbf{R}' , the p - B relative coordinate), and ϕ_{nA} is the bound state for the final n - A system. The difference $(U_{pA} - U_{pB})$ is called the *remnant term*, which is sometimes neglected for convenience. It should be stressed that, in the case of exotic nuclei, it can be very significant. In our study it is always included.

B. The Faddeev-AGS method

The Faddeev formalism explicitly includes the deuteron $d + A$, the proton (nA) + p , and the neutron (pA) + n components. Three sets of Jacobi variables are used such that each component is treated in its proper basis. In the AGS approach the three-particle scattering is described in terms of the transition operators $T_{\beta\alpha}$, where α (β) corresponds to the initial (final) channel in the odd-man-out notation. The transition operators obey the AGS equations [8] that are a system of coupled integral equations

$$T_{\beta\alpha} = \bar{\delta}_{\beta\alpha} G_0^{-1} + \sum_{\gamma=1}^3 \bar{\delta}_{\beta\gamma} t_{\gamma} G_0 T_{\gamma\alpha}. \quad (9)$$

Here $\bar{\delta}_{\beta\alpha} = 1 - \delta_{\beta\alpha}$ and $G_0 = (E + i0 - H_0)^{-1}$ is the free resolvent with E being the total energy in the three-body c.m. system. The two-body transition operator for each interacting pair is derived from the pair potential v_γ via the Lippmann-Schwinger equation

$$t_\gamma = v_\gamma + v_\gamma G_0 t_\gamma. \quad (10)$$

The scattering amplitude $X_{\beta\alpha}$ is the on-shell matrix element of $T_{\beta\alpha}$ calculated between initial and final channel states as

$$X_{\beta\alpha} = \langle \phi_\beta | T_{\beta\alpha} | \phi_\alpha \rangle. \quad (11)$$

In the case of elastic scattering $\beta = \alpha$, while $\beta = 0$ for breakup and $0 \neq \beta \neq \alpha$ for transfer reactions. The AGS equations (9) are solved in momentum space using partial wave decomposition. The proton-nucleus Coulomb interaction is treated using the method of screening and renormalization [10,11]. Further numerical details can be found in Refs. [23–26].

III. NUMERICAL DETAILS AND INPUTS

In this section we present the pair interactions necessary to define the three-body Hamiltonian as well as some details for the model space used. Both CDCC and Faddeev-AGS are computationally expensive; thus, without sacrificing the final goal, we make simplifications to the $p + n + A$ system. To reduce the number of channels, we have neglected the spins of the particles and thus all the spin-orbit terms in the interactions are not included. Also, a single Gaussian interaction is used to describe the deuteron and its continuum [27],

$$V(r) = -V_0 e^{-(r/r_0)^2}, \quad (12)$$

with $V_0 = 72.15$ MeV and $r_0 = 1.484$ fm. The potential reproduces the binding energy of deuteron and low-energy p - n 3S_1 phase shifts but fails heavily in other partial waves. While the comparison of CDCC and Faddeev-AGS is meaningful given that the same Hamiltonian is used in both formulations, a direct comparison of the predicted cross sections with data should be avoided. We have chosen for all our test cases energies at which data exist and thus this study retains its relevance to experiments.

An important ingredient of the three-body Hamiltonian, the nucleon-nucleus optical potentials, are all taken from the global parametrization CH89 [28]. The optical potentials are energy dependent and should be considered within the context of the reaction model. In CDCC calculations, U_{pA} and U_{nA} are calculated at half the deuteron incident energy $E_d/2$, while the auxiliary potential, U_{pB} , is calculated at the proton energy E_p corresponding to the exit channel. The Faddeev-AGS calculations with exactly the same choice of U_{pA} and U_{nA} as in CDCC yield results for elastic and breakup observables only, as there is no transfer channel with complex U_{nA} . We therefore perform also the Faddeev-AGS calculations where a real neutron-nucleus potential is used in the partial wave corresponding to the final bound state. The same interaction is used to produce the neutron-nucleus bound state ϕ_{nA} in Eq. (8). We take a Woods-Saxon central potential with standard geometry: radius $r_0 = 1.25$ fm and diffuseness $a = 0.65$ fm.

TABLE I. Parameters of the n - A binding potential used in the calculations. The radius and the diffuseness are taken to be $r_0 = 1.25$ fm and $a_0 = 0.65$ fm, respectively. S_n is the neutron separation energy, V_{nA} is the depth of the n - A binding potential, and nl are the quantum numbers describing the ground state of the nucleus $B = A + n$.

Nucleus (A)	nl	S_n (MeV)	V_{nA} (MeV)
^{10}Be	$2s$	0.504	57.064
^{12}C	$1p$	4.947	39.547
^{48}Ca	$2p$	5.146	48.905

The depths are adjusted to reproduce the neutron separation energy of the relevant state. Details are given in Table I.

For both CDCC and Faddeev-AGS, convergence needs to be studied in detail. While elastic and transfer observables offered a minor challenge from the point of view of convergence, the same cannot be said of breakup distributions. Even though spins were neglected to reduce computational cost, breakup calculations proved to be at the limit of our numerical capabilities. Due to technical difficulties in the Faddeev-AGS, breakup calculations were performed without the Coulomb interaction. In Sec. III A we present the CDCC model space based on transfer observables. For those cases in which the model space was insufficient to ensure convergence of the breakup cross sections, the predictions are presented with bands instead of lines, estimated on the convergence behavior with increasing l . In Sec. III B we present the Faddeev-AGS model space chosen to ensure convergence of all calculated observables.

A. CDCC model space

The $^{10}\text{Be}(d, p)^{11}\text{Be}$ reaction is studied at three beam energies, $E_d = 21.4, 40.9,$ and 71 MeV. The calculations include p - n partial waves up to $l_{\max} = 4$ and $Q_{\max} = 4$ multipoles in the expansion of the coupling potentials. The coupled equations are integrated up to $R_{\max} = 60$ fm with total angular momentum $J_{\max} = 40$ for $E_d = 21.4$ MeV and $J_{\max} = 50$ for $E_d = 40.9$ and 71 MeV.

Calculations for the $^{12}\text{C}(d, p)^{13}\text{C}$ reaction include p - n partial waves $l \leq 6$ and coupling potentials expanded up to $Q_{\max} = 6$. The coupled equations are integrated up to $R_{\max} = 60$ fm with $J_{\max} = 30$ for $E_d = 12$ MeV and $J_{\max} = 50$ for $E_d = 56$ MeV.

Calculations for the $^{48}\text{Ca}(d, p)^{49}\text{Ca}$ reaction include p - n partial waves $l \leq 6$ and coupling potentials expanded up to $Q_{\max} = 6$. The coupled equations are integrated up to $R_{\max} = 80$ fm with $J_{\max} = 70$ for $E_d = 56$ MeV.

For all calculations, the radial integration was performed in steps of 0.06 fm and the momentum average defining the bins was performed on a mesh with 20 points. The schematic detail of the bin structure used for the discretized deuteron continuum in these calculations, is shown in Fig. 1.

When considering transfer, in addition to the above mentioned model space, the nonlocality of the transfer kernel needs to be considered. The details of the nonlocal parameters used are presented in Table II. Due to the strong repulsive couplings

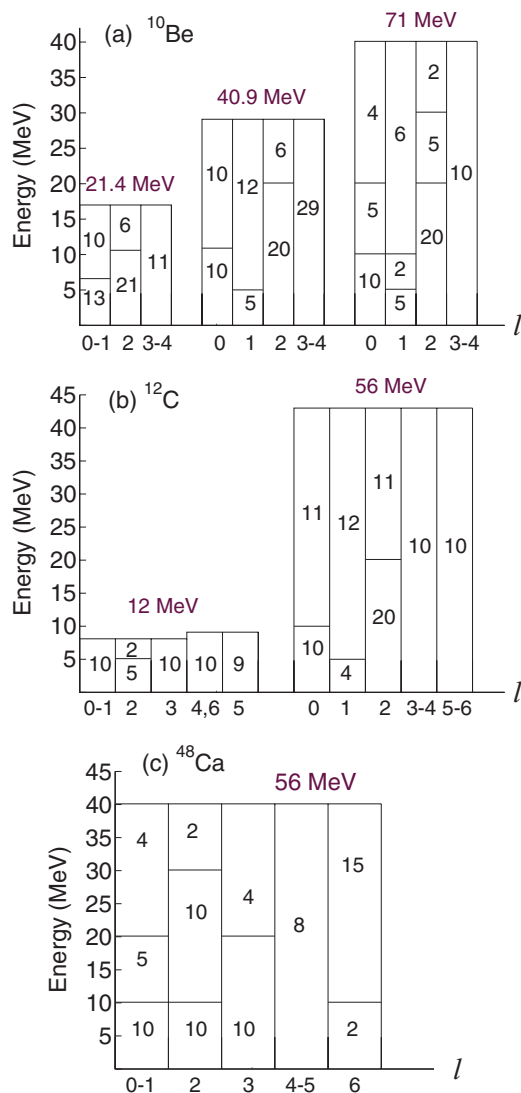


FIG. 1. (Color online) Schematic detail of the deuteron continuum used in the CDCC calculations, showing the number of bins and the energy range as a function of l : (a) $d+^{10}\text{Be}$, (b) $d+^{12}\text{C}$, and (c) $d+^{48}\text{Ca}$.

at short distances, for $^{10}\text{Be}(d, p)^{11}\text{Be}$ at $E_d = 71$ MeV, it was necessary to introduce an L -dependent internal cut in the couplings.

B. Faddeev-AGS model space

The AGS equations are solved using partial wave decomposition. However, in contrast to CDCC, three bases corresponding to the three choices of Jacobi momenta are used. The maximum we include for the p - n partial waves is $l_{\max} = 5$. For the ^{10}Be target, n - ^{10}Be partial waves up to $l_{\max} = 8$ and p - ^{10}Be partial waves up to $l_{\max} = 16$ are included. For the ^{12}C target, n - ^{12}C partial waves up to $l_{\max} = 8$ and p - ^{12}C partial waves up to $l_{\max} = 18$ are included. For the ^{48}Ca target, n - ^{48}Ca partial waves up to $l_{\max} = 10$ and p - ^{48}Ca partial waves up to $l_{\max} = 20$ are included. The maximal total angular momentum considered is $J_{\max} = 60$. Depending on

TABLE II. Parameters of the nonlocal transfer kernel used in the CDCC calculations (details can be found in Ref. [29]).

Target	E_d (MeV)	Centration(fm)	Nonlocal width (fm)
^{10}Be	21.4	2.16	14
	40.9	1.92	20
	71	1.32	12
^{12}C	12	-0.96	6
	56	-0.66	7
^{48}Ca	56	-0.78	7

reaction and energy, some of these cutoffs can be reduced without affecting the quality of the results. The integrals are discretized using Gaussian quadrature rules with about 50 grid points for each Jacobi momentum. The Coulomb screening radius is $R_C = 16$ fm. The results are well converged except for the breakup cross sections at small angles. In that case a special treatment of the pure Coulomb breakup term as described in Ref. [12] improves the convergence. However, even with this special treatment including $R_C = 50$ fm and proton-nucleus partial waves up to $l_{\max} = 40$, we were unable to get better than 20% accuracy for small angles (i.e., $\theta < 15^\circ$). We therefore present breakup results neglecting the Coulomb force, since the main goal of the present work is the comparison of the methods and not the analysis of experimental data. The Faddeev-AGS calculations without the Coulomb force are well converged; in this case $l_{\max} = 10$ for p - A partial waves is sufficient.

IV. RESULTS AND DISCUSSION

In this section we present results for elastic scattering, transfer, and breakup. For many of the chosen cases, data is available. However, because we neglect spin, a direct comparison with data is not appropriate. It is the comparison between the methods that is meaningful.

While the reference calculations are performed with the neutron and proton optical potentials calculated at half the deuteron energy, there are small useful variations in the interactions that should be considered carefully. For clarity we describe the various labels that will appear in the following subsections in Table III. For elastic scattering and breakup, the standard CDCC and Faddeev-AGS calculations are labeled CDCC and FAGS, respectively. These take the nucleon optical potentials U_{pA} and U_{nA} at half the deuteron energy in all

TABLE III. Types of Faddeev-AGS calculations being performed, the labels used, the energies at which the associated interactions were determined, and whether or not a neutron-nucleus potential supports a bound state.

Label	U_{pA}	U_{nA}	nA -bound
FAGS	$E_d/2$	$E_d/2$	no
FAGS1	$E_d/2$	$E_d/2$	yes
FAGS2	E_p	$E_d/2$	yes

partial waves and therefore produce no bound states in the nucleon-nucleus subsystems.

For there to be a transfer channel in Faddeev-AGS, the relevant interaction needs to hold a bound state. The only difference between FAGS and FAGS1 is the inclusion of a neutron-nucleus bound state (by taking a real interaction for the nA subsystem in the partial wave for which a bound state exists). Comparing FAGS and FAGS1 for elastic and breakup reactions tells us about the importance of coupling to the transfer channel.

In evaluating transfer matrix elements, the calculations labeled CDCC take the nucleon-nucleus interactions (U_{pA}, U_{nA}) in the initial state to be at half the deuteron energy $E_d/2$ and the auxiliary interaction U_{pB} to be at the proton energy in the exit channel E_p , closely mimicking the physical process. Therefore it makes sense to consider also the Faddeev-AGS counterpart FAGS2, where U_{pA} is determined at E_p . We note that FADD2 and FADD of Refs. [15,16] correspond to our FAGS1 and FAGS2, respectively. For completeness we also explore the effect of this subtle difference in the initial Hamiltonian in CDCC, by performing CDCC2 (where all proton optical potentials are calculated at E_p , including the one in the incoming channel).

A. Elastic scattering

The simplest reaction to study is elastic scattering. The elastic differential cross section is sensitive to the asymptotic behavior of the three-body wave function in a very particular region of phase space, namely when the neutron and proton are bound. It is thus one basic test for a complete reaction theory.

The elastic cross sections for deuterons on ^{10}Be , ^{12}C , and ^{48}Ca are shown in Figs. 2, 3, and 4, respectively. Plotted are the standard CDCC (dashed) and FAGS (solid) angular distributions, as well as the results of FAGS1 (dotted circles), when the transfer channel is included. The differential cross section is divided by the corresponding Rutherford cross section to allow for inspection at larger angles. Overall CDCC and FAGS agree, with exception of $d+^{12}\text{C}$ at 12 MeV, where some discrepancy is found beyond 40° . The inclusion of the transfer couplings has a minor effect, as can be seen by comparing FAGS and FAGS1, which produces only small modifications in the distributions, mainly at large angles.

B. Transfer reaction

Contrary to elastic scattering, the transfer process is typically sensitive to the three-body scattering wave function at the surface of the target, and therefore poses different challenges for reaction theory. Here, all cases refer to transfer to the ground state (g.s.) of the final nucleus.

In Fig. 5, we present the angular distribution for the $^{10}\text{Be}(d,p)^{11}\text{Be}$ reaction calculated at $E_d = 21.4, 40.9,$ and 71 MeV, respectively. We first compare the standard CDCC (dashed) and standard FAGS1 (solid). We observe that, at $E_d = 21.4$ MeV, the two methods are in perfect agreement, but significant discrepancies appear at higher beam energy. To determine how much of those discrepancies can be attributed to the choice of the energy at which the optical potentials are evaluated, it is useful to consider the auxiliary

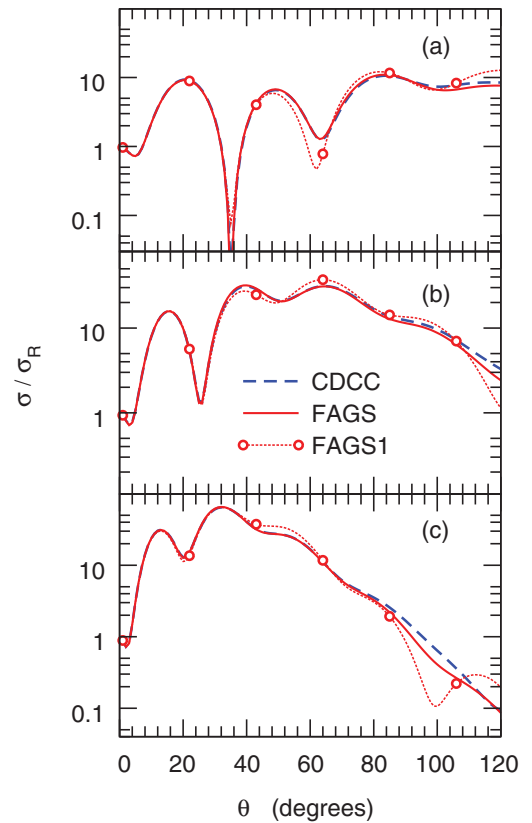


FIG. 2. (Color online) Elastic cross section for $d+^{10}\text{Be}$: (a) $E_d = 21.4$ MeV, (b) $E_d = 40.9$ MeV, and (c) $E_d = 71$ MeV.

calculations CDCC2 (dotted diamonds) and FAGS2 (dotted circles). Comparing FAGS2 and CDCC2 (both with U_{pA} at E_p in the entrance channel) one concludes that the discrepancy is almost independent of the ambiguity in U_{pA} . As in Ref. [16] we do find an increasing dependence on the choice of the optical

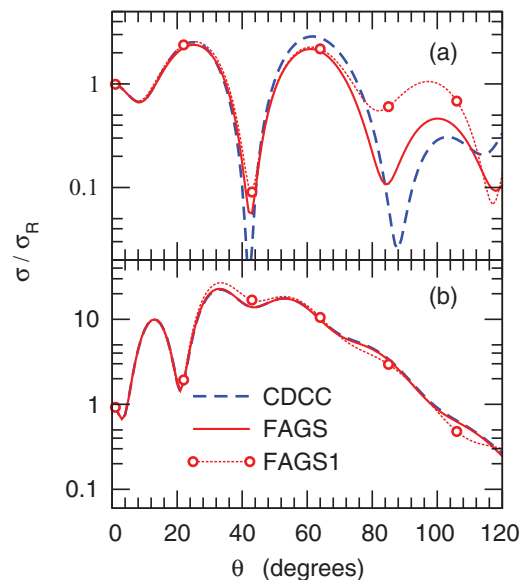


FIG. 3. (Color online) Elastic cross section for $d+^{12}\text{C}$: (a) $E_d = 12$ MeV and (b) $E_d = 56$ MeV.

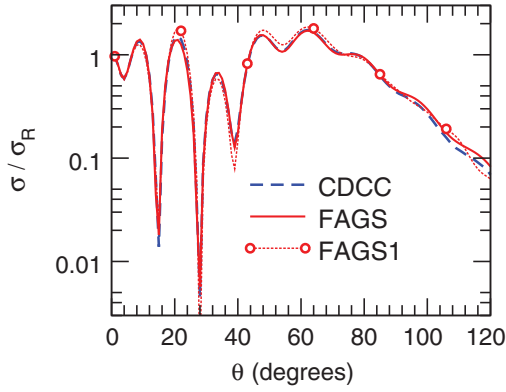


FIG. 4. (Color online) Elastic cross section for $d+^{48}\text{Ca}$ at $E_d = 56$ MeV.

potentials with beam energy. CDCC calculations should be independent of the choice of the auxiliary interaction. This is true for the lowest energy, but a few percent discrepancy starts to appear as the beam energy increases.

In Fig. 6, we show $d\sigma/d\Omega$ for the $^{12}\text{C}(d, p)^{13}\text{C}$ reaction at $E_d = 12$ and 56 MeV. Just as in the case of ^{10}Be , the CDCC predictions for (d, p) on ^{12}C at low energy provide a very good approximation to the Faddeev solution (FAGS1). However, the disagreement at 56 MeV becomes significant (around 20%).

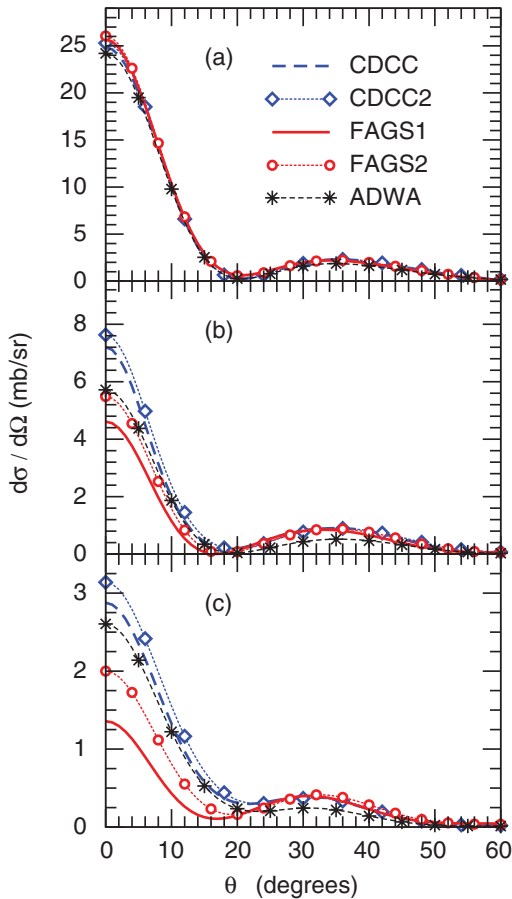


FIG. 5. (Color online) Angular distribution for $^{10}\text{Be}(d, p)^{11}\text{Be}$: (a) $E_d = 21.4$ MeV, (b) $E_d = 40.9$ MeV, and (c) $E_d = 71$ MeV.

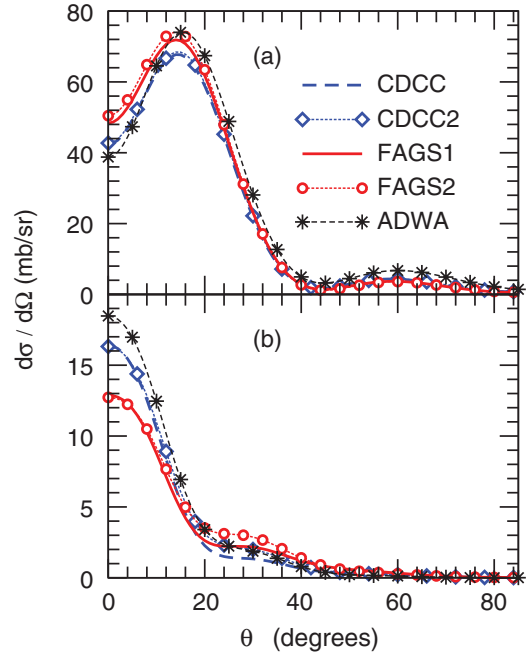


FIG. 6. (Color online) Angular distribution for $^{12}\text{C}(d, p)^{13}\text{C}$: (a) $E_d = 12$ MeV and (b) $E_d = 56$ MeV.

Whereas in ^{10}Be there was a strong dependence of the transfer cross section on the choice of the energy at which the optical potentials are evaluated, for ^{12}C , no such dependence exists (compare FAGS1 and FAGS2 or CDCC and CDCC2) and therefore the disagreement is quantitatively robust.

In Fig. 7 we present the angular distributions following (d, p) transfer to the ground state of ^{49}Ca at 56 MeV. Small but not negligible discrepancies are found in the shapes of $d\sigma/d\Omega$ between FAGS1 and CDCC, accompanied by a significant dependence on the optical potential (FAGS2 and CDCC2), which makes the comparison ambiguous.

We connect the present work with the comparative study [16] between the finite-range adiabatic wave approximation (ADWA) method and Faddeev-AGS. For that purpose, we include in Figs. 5–7 the finite-range ADWA predictions

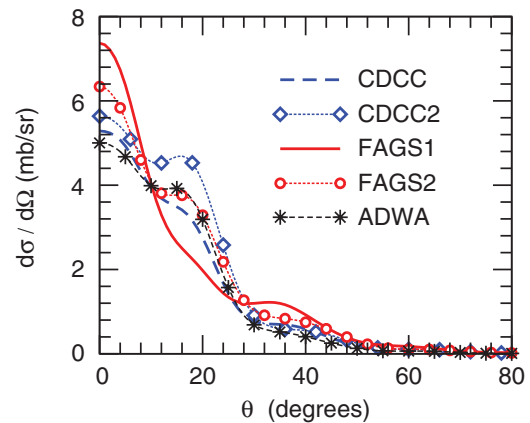


FIG. 7. (Color online) Angular distribution for $^{48}\text{Ca}(d, p)^{49}\text{Ca}$ at $E_d = 56$ MeV.

TABLE IV. Percentage differences between the (d, p) cross sections at the peak of the angular distribution predicted by the various methods, for the three targets here considered, as a function of beam energy E_d .

Target	E_d (MeV)	Δ_{A-C} (%)	Δ_{F-C} (%)	Δ_{F-A} (%)
^{10}Be	21.4	-3	3 ± 1	6 ± 1
	40.9	-21	-36 ± 19	-19 ± 19
	71.0	-9	-53 ± 47	-48 ± 47
^{12}C	12.0	8	6 ± 3	-2 ± 3
	56.0	13	-21 ± 1	-30 ± 1
^{48}Ca	56.0	-5	39 ± 14	47 ± 14

(short-dashed stars). These correspond to exactly the same Hamiltonian as the CDCC calculations performed here, and therefore differ from those in Ref. [16]. Encouragingly, for the reactions on ^{10}Be , ADWA performs just as well or even better than CDCC. Figure 5 is further evidence that, for $l = 0$ transfer, ADWA provides a very good approximation to Faddeev-AGS for reactions around 10 MeV/u, as concluded in Ref. [16]. For ^{12}C and ^{48}Ca , ADWA cross sections differ from the CDCC predictions by a few percent, usually increasing the discrepancy with the FAGS1 results (as compared to CDCC).

Table IV provides a quantitative estimate for the discrepancy between the various methods here considered. We provide percentage differences of the differential cross sections at the peak of the angular distributions: (i) Δ_{A-C} compares ADWA with the standard CDCC, relative to CDCC, (ii) Δ_{F-C} compares FAGS1 with CDCC, relative to CDCC, and (iii) Δ_{F-A} compares FAGS1 with adiabatic, relative to ADWA. The error in Δ_{F-C} and Δ_{F-A} is estimated from the percentage difference obtained with FAGS2 versus FAGS1.

C. Deuteron breakup

In this section, we compare CDCC angular and energy distributions following the breakup of the deuteron with the Faddeev-AGS counterparts. We consider FAGS and FAGS1, i.e., without and with a bound state in the nA subsystem.

Breakup calculations are computationally more demanding than transfer or elastic ones. As mentioned in Sec. III B, the Faddeev-AGS breakup results obtained with the present technical implementation are not sufficiently accurate at forward angles when the Coulomb force is included. For this reason, the comparison of breakup cross sections is performed switching off the Coulomb interaction in both CDCC and Faddeev-AGS.¹

In its present implementation, CDCC breakup observables are reconstructed from the asymptotic form of the three-body wave function. This implies that the asymptotics of the three-body wave function needs to be good not only when the neutron and proton are close to each other, but also when they are far apart. This poses considerable challenges to our numerical methods. For all the CDCC calculations, we went to the

¹Based on CDCC predictions, the inclusion of the Coulomb interaction can increase the cross section by up to a factor of 2.

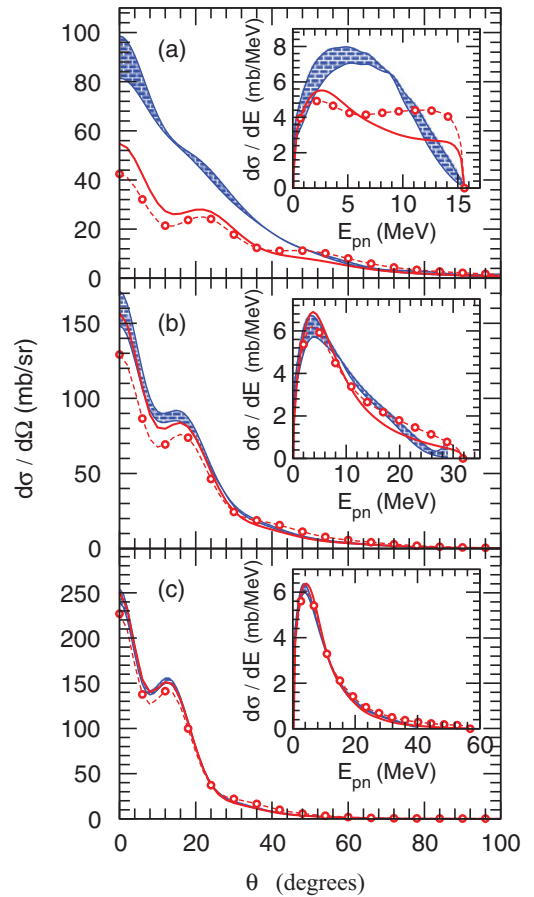


FIG. 8. (Color online) Breakup distributions for the $^{10}\text{Be}(d, pn)^{10}\text{Be}$ reaction at (a) $E_d = 21$ MeV, (b) $E_d = 40.9$ MeV, and (c) $E_d = 71$ MeV. Results for CDCC (hatched band), FAGS (solid), and FAGS1 (circles).

numerical limit of the methods, mostly dictated by the number of partial waves included in the deuteron continuum. For the nuclear-only CDCC breakup calculations, $Q_{\max} = l_{\max} = 6$ was our model space limit. The error bands in the CDCC cross sections are due to the truncation of the model space, and have been extrapolated from the differences found in the cross sections for $Q_{\max} = l_{\max} = 6$ and $Q_{\max} = l_{\max} = 4$. Typically the calculations at higher energies have a smaller error bar because for those energies the effect of these higher multipole couplings is smaller.

In Fig. 8 we present the results for the angular distribution as a function of the c.m. angle of the pn system following the breakup on ^{10}Be at the three energies of choice. The hatched band, the solid line, and the circles correspond to CDCC, FAGS, and FAGS1 predictions, respectively. At the lowest energy, we find that CDCC does not reproduce FAGS, even taking into account the error estimated by model space truncation. At the higher energies, this discrepancy is removed. The insets of Fig. 8 contain the corresponding energy distributions as functions of the proton-neutron relative energy E_{pn} . Again, a very large discrepancy is found at 21.4 MeV while fair agreement between CDCC and FAGS is obtained at the higher energies.

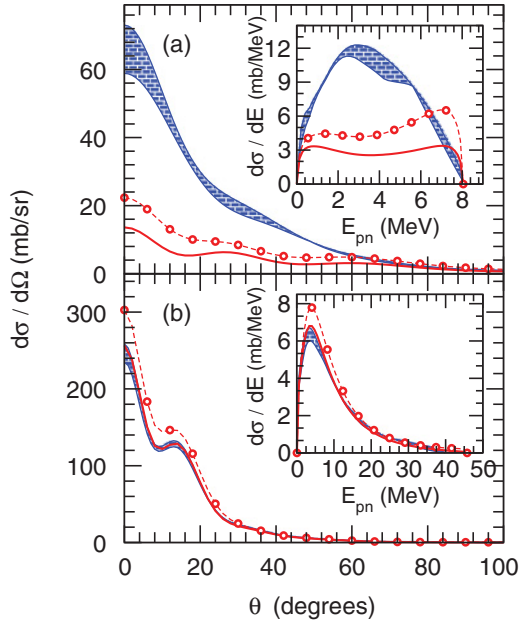


FIG. 9. (Color online) Breakup distributions for the $^{12}\text{C}(d, pn)^{12}\text{C}$ reaction at (a) $E_d = 12$ MeV and (b) $E_d = 56$ MeV. Results for CDCC (hatched band), FGS (solid), and FGS1 (circles).

Similar conclusions can be drawn from the comparison of breakup angular and energy distributions for reactions on ^{12}C (Fig. 9). Despite the large error bar in the CDCC predictions, there is a striking mismatch between CDCC and FGS in both magnitude and shape of the breakup cross sections at 12 MeV. These discrepancies disappear at the higher energy. Agreement is obtained between CDCC and FGS for the breakup of deuterons on ^{48}Ca at 56 MeV, as shown in Fig. 10. The effects of including the nA bound state in the transfer channel is shown with FGS1 (dotted circles). By comparing FGS and FGS1 we conclude that the effects of transfer are not negligible on breakup, particularly at low energies.

Although for transfer we found excellent agreement for all reactions at low energy (≈ 10 MeV/u), for breakup it is exactly at the low energy that CDCC appears to break down. To better understand this, we have investigated the relevant

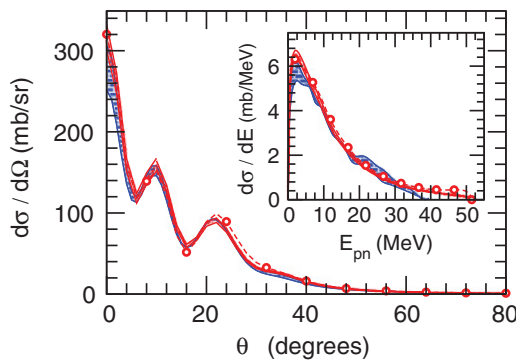


FIG. 10. (Color online) Breakup distributions for the $^{48}\text{Ca}(d, pn)^{48}\text{Ca}$ reaction at $E_d = 56$ MeV. Results for CDCC (hatched band), FGS (solid), and FGS1 (circles).

contributions to the breakup cross sections within FGS. In particular, we wanted to understand the relative importance of the three Faddeev components, namely the deuteron channel, the proton channel, and the neutron channel, in evaluating the breakup observables. We suspected this was the key to understanding the discrepancies between CDCC and FGS, because CDCC is based on an expansion in the deuteron channel alone. Even though in the FGS calculations there are no bound states in the proton and the neutron channels (U_{nA} and U_{pA} contain an imaginary term), the breakup is still distributed between all three Faddeev components. We find that, for breakup at low beam energies, the proton and neutron Faddeev components are equally important as the deuteron component, and there are destructive interferences between the various components, at most values of E_{pn} , that reduce the cross section significantly.

At the limiting case where all the energy is in the proton-neutron relative motion, the phase space factor goes as $\sim q_A \sim \sqrt{E_{pn}^{\max} - E_{pn}}$, where q_A is the target recoil momentum in the c.m. system. This is not well reproduced when expanding in terms of a truncated deuteron basis, as in CDCC. Given the coordinate choice, it is expected that the asymptotic behavior of the CDCC wave function is at its best when the proton and neutron are close to each other, but not in the opposite case. The results presented in Figs. 8–10 are a manifestation of this fact. CDCC breaks down in the lower energy regime, where we find broader angular and energy distributions and there are larger contributions to the breakup cross section from $E_{pn} \approx E_{pn}^{\max}$.

Our previous work [18] suggested that the discrepancies between CDCC and Faddeev in breakup arrived as a consequence of the existence of a bound state in the rearrangement channel. Results shown in Figs. 8 and 9 demonstrate this is not always the case. Even if there is no nA bound state, large discrepancies can occur at low energies. The inclusion of a bound state enhances the disagreement, as shown by FGS1 results in Figs. 8–10.

D. Sensitivity to interactions

As pointed out before, in Secs. IV A–IV C we have neglected nucleon spin to reduce the computational cost of the study, and a simple Gaussian interaction was used for the nucleon-nucleon (NN) interaction. However it is important to understand the magnitude of the effect of this simplification, particularly if one is interested in comparing to data.

The sensitivity of the breakup observables to details of the NN interaction was studied for ^{11}Be on protons at 63.7 MeV/u in Ref. [30]. In this study, Faddeev-AGS calculations using a Gaussian NN potential were compared with those using the realistic CD-Bonn NN potential [31]. It was observed that the breakup observables were very sensitive to the description of the p waves where our single Gaussian NN potential fails completely.

Here, we focus on transfer and elastic scattering. We repeat FGS1 calculations using the realistic CD-Bonn potential for scattering of the deuteron on ^{12}C , first excluding the spin-orbit force in the optical potential, and next including it. In Figs. 11 and 12 we show the angular distribution for $^{12}\text{C}(d, p)^{13}\text{C}$ reaction at $E_d = 12$ and 56 MeV. The red dashed

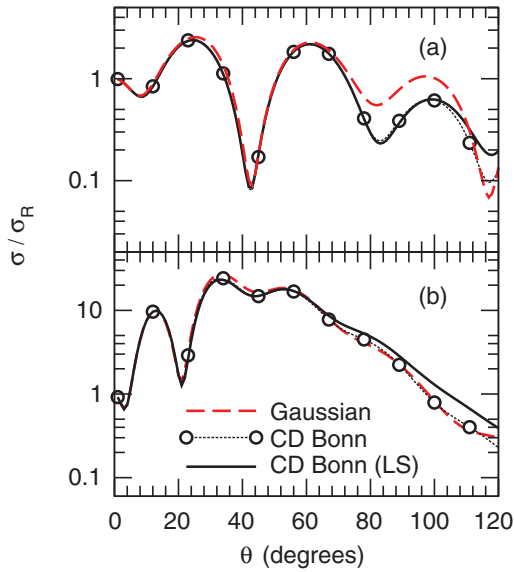


FIG. 11. (Color online) Elastic distributions for FAGS1 calculations for the $^{12}\text{C}(d, d)^{12}\text{C}$ reaction at (a) $E_d = 12$ MeV and (b) $E_d = 56$ MeV.

line corresponds to our standard calculation, using a single Gaussian for the NN interaction, and neglecting the spin-orbit force in the optical potentials. The open circles correspond to the FAGS1 calculation using the CD-Bonn potential for the NN interaction, still neglecting the spin-orbit force in the optical potentials. And finally, the black solid line includes the CD-Bonn potential for the NN interaction and the appropriate spin-orbit terms in the optical potentials. Note that the FAGS1 transfer cross section in Fig. 12 differs by a statistical factor

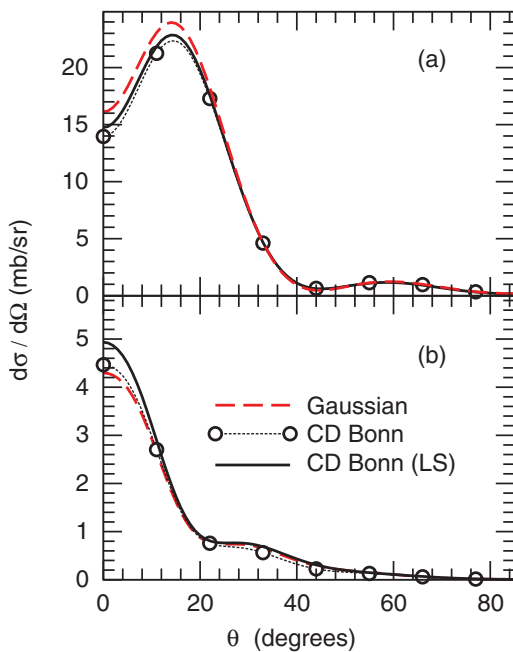


FIG. 12. (Color online) Transfer angular distributions for FAGS1 calculations for the $^{12}\text{C}(d, p)^{13}\text{C}$ reaction at (a) $E_d = 12$ MeV and (b) $E_d = 56$ MeV.

from that in Fig. 6, because here the spin of the deuteron is correctly included.

The elastic cross sections are insensitive to the choice of potentials except for backward angles, the effect being more noticeable at lower energy. Transfer cross sections are modified by a few percent when including a realistic NN interaction for the reaction at low energy, while at higher energy the cross section is not affected by details of the NN interaction. As to the effect of the spin-orbit term in the nucleon optical potentials, the effect is only significant at high energy. Overall the effects are small and confirm the relevance of this study to experiment.

V. SUMMARY AND CONCLUSIONS

In this study we perform a systematic comparison between CDCC and Faddeev-AGS methods for deuteron-induced reactions. The CDCC formalism under study here corresponds to the standard method introduced in Ref. [6], and is based on a truncated expansion on the deuteron continuum. The Faddeev-AGS method considered in this work corresponds to the solution of the AGS equations [8], including Coulomb screening and renormalization as in Ref. [11]. For all practical purposes, Faddeev-AGS solutions are considered exact and therefore this study should serve as a test of the reliability of CDCC.

We focus on deuteron reactions on ^{10}Be , ^{12}C , and ^{48}Ca , including a wide range of beam energies. We compute elastic scattering, transfer cross sections to the ground state of the final system, as well as breakup observables. In CDCC, elastic scattering and breakup cross sections are obtained directly from the S matrix, while transfer is calculated replacing the exact three-body wave function with the CDCC wave function in the exact post-form T matrix.

Our CDCC/FAGS comparisons show no immediate correlation between elastic scattering, transfer, or breakup. In other words, finding agreement for the elastic scattering for a given target and beam energy does not imply agreement in breakup or transfer. Indeed, these processes are sensitive to different parts of configuration space and therefore, only by looking at elastic scattering, transfer, and breakup simultaneously, can the CDCC method be thoroughly tested.

Overall, and regardless of the beam energy, CDCC is able to provide a good approximation to FAGS for elastic scattering. The inclusion of a neutron-nucleus bound state in the FAGS1 calculations introduces small modifications mostly at backward angles. Only for $d+^{12}\text{C}$ at 12 MeV did we find stronger discrepancies in the elastic angular distribution between CDCC and Faddeev-AGS.

The comparison of CDCC and Faddeev-AGS for transfer cross sections is consistent with the results presented in Ref. [16]. We found CDCC to be a very good approximation of FAGS1 at reactions around 10 MeV/u, but not so good for higher beam energies.

As opposed to transfer, breakup observables predicted by CDCC are at their best for the higher beam energies explored in this work. To reduce the technical challenges of the problem, we ignore the Coulomb interaction in the breakup comparison. Also, we use exactly the same Hamiltonian (CDCC and FAGS)

to remove any ambiguity. Taking into account the estimated error due to the truncation of the model space in the CDCC calculations, CDCC predictions for the breakup, angular and energy distributions are in good agreement with FAGS for all but the lowest energies considered. For deuteron breakup on ^{10}Be at 21.4 MeV and on ^{12}C at 12 MeV, CDCC fails. Strong contributions from the proton and neutron Faddeev components, not explicitly included in the CDCC expansion, are present when the proton-neutron relative energies are large. At low energy, the energy distribution is broad, the breakup to scattering states with large proton-neutron relative energy is important, and therefore CDCC does not perform well. One possible solution to this shortcoming is to use the CDCC wave function in a T matrix that probes only short distances between the proton and neutron, instead of its asymptotic form.

The present comparisons pose important constraints on the validity of CDCC when applied to deuteron-induced reactions. However, it is critical to realize that the number of reactions which can be calculated with the present implementation of Faddeev-AGS is more limited. Indeed, as the mass of the target increases, Coulomb effects become stronger, requiring larger screening radius and more partial waves; this renders the solution of the AGS equations in the partial-wave representation impossible. In addition, the Pade summation technique used to solve the AGS equations converges slower at low energies (10 MeV/u) and for large A where optical potentials are strong

but the absorption is weak; with the present interaction model we were unable to obtain converged solutions for $A = 48$ at $E_d = 19.3$ MeV. It would be desirable to extend present techniques used in Faddeev-AGS or to develop new methods which can overcome these difficulties.

Finally, one should keep in mind that this work is based on a pure three-body formulation of deuteron-induced reactions. This assumes that the final bound state populated in the (d, p) reaction is of pure single particle nature. A great challenge and important advance for the Faddeev-AGS formulation is the inclusion of degrees of freedom of the target, which is necessary for a more realistic description of the process.

ACKNOWLEDGMENTS

We thank Ron Johnson and the members of the TORUS collaboration for important discussions on this work. We are in debt to Ian Thompson for his invaluable support with FRESKO. The work of N.J.U. was supported by the Department of Energy topical collaboration Grant No. DE-SC0004087. The work of A.D. was partially supported by the FCT Grant No. PTDC/FIS/65736/2006. The work of F.M.N. was partially supported by the National Science Foundation Grant No. PHY-0800026 and the Department of Energy through Grant No. DE-FG52-08NA28552.

-
- [1] M. Thoennessen and B. Sherrill, *Nature (London)* **473**, 25 (2011).
 - [2] S. K. Kubono, in *Nuclear Physica in the 21st Century: International Nuclear Physics Conference INPC 2001*, edited by E. Norman, L. Schroeder, G. Wozniak, and A. M. Smith, AIP Conf. Proc. No. 610 (AIP, New York, 2002), p. 132.
 - [3] A. Mukhamedzhanov *et al.*, *Phys. Rev. C* **84**, 024616 (2011).
 - [4] R. C. Johnson and P. J. R. Soper, *Phys. Rev. C* **1**, 976 (1970).
 - [5] R. C. Johnson and P. C. Tandy, *Nucl. Phys. A* **235**, 56 (1974).
 - [6] N. Austern, Y. Iseri, M. Kamimura, M. Kawai, G. Rawitsher, and M. Yahiro, *Phys. Rep.* **154**, 125 (1987).
 - [7] L. D. Faddeev, *Zh. Eksp. Theor. Fiz.* **39**, 1459 (1960) [*Sov. Phys. JETP* **12**, 1014 (1961)].
 - [8] E. O. Alt, P. Grassberger, and W. Sandhas, *Nucl. Phys. B* **2**, 167 (1967).
 - [9] W. Glöckle, *The Quantum Mechanical Few-Body Problem* (Springer-Verlag, Berlin, 1983).
 - [10] E. O. Alt and W. Sandhas, *Phys. Rev. C* **21**, 1733 (1980).
 - [11] A. Deltuva, A. C. Fonseca, and P. U. Sauer, *Phys. Rev. C* **71**, 054005 (2005).
 - [12] A. Deltuva, A. M. Moro, E. Cravo, F. M. Nunes, and A. C. Fonseca, *Phys. Rev. C* **76**, 064602 (2007).
 - [13] A. Deltuva, *Phys. Rev. C* **79**, 021602(R) (2009); **79**, 054603 (2009).
 - [14] N. B. Nguyen, F. M. Nunes, and R. C. Johnson, *Phys. Rev. C* **82**, 014611 (2010).
 - [15] F. M. Nunes, A. Deltuva, and J. Hong, *Phys. Rev. C* **83**, 034610 (2011).
 - [16] F. M. Nunes and A. Deltuva, *Phys. Rev. C* **84**, 034607 (2011).
 - [17] F. M. Nunes, *Scholarpedia* **6**, 10497 (2011).
 - [18] A. M. Moro, R. Crespo, F. M. Nunes, and I. J. Thompson, *Phys. Rev. C* **66**, 024612 (2002); **67**, 047602 (2003).
 - [19] K. Ogata, M. Yahiro, Y. Iseri, and M. Kamimura, *Phys. Rev. C* **67**, 011602(R) (2003).
 - [20] H. B. Jeppesen *et al.*, *Phys. Lett. B* **642**, 449 (2006).
 - [21] N. Keeley and R. S. Mackintosh, *Phys. Rev. C* **77**, 054603 (2008).
 - [22] Ian Thompson and Filomena Nunes, *Nuclear Reactions for Astrophysics* (Cambridge University Press, Cambridge, 2009).
 - [23] K. Chmielewski, A. Deltuva, A. C. Fonseca, S. Nemoto, and P. U. Sauer, *Phys. Rev. C* **67**, 014002 (2003).
 - [24] A. Deltuva, K. Chmielewski, and P. U. Sauer, *Phys. Rev. C* **67**, 034001 (2003).
 - [25] A. Deltuva, A. C. Fonseca, and P. U. Sauer, *Phys. Rev. C* **72**, 054004 (2005); **73**, 057001 (2006).
 - [26] A. Deltuva, *Phys. Rev. C* **74**, 064001 (2006).
 - [27] M. Yahiro, Y. Iseri, M. Kamimura, and M. Nakano, *Phys. Lett. B* **141**, 19 (1984).
 - [28] R. L. Varner *et al.*, *Phys. Rep.* **201**, 57 (1991).
 - [29] I. J. Thompson, *Comput. Phys. Rep.* **7**, 167 (1988).
 - [30] E. Cravo, R. Crespo, A. M. Moro, and A. Deltuva, *Phys. Rev. C* **81**, 031601(R) (2010).
 - [31] R. Machleidt, *Phys. Rev. C* **63**, 024001 (2001).